Proceedings of the ASME 2010 3rd Joint US-European Fluids Engineering Summer Meeting and 8th International Conference on Nanochannels, Microchannels, and Minichannels
FEDSM-ICNMM2010
August 1-5, 2010, Montreal, Canada

FEDSM-ICNMM2010-30814

HYPERCHAOTIC BEHAVIOUR OF SHELLS SUBJECTED TO FLOW AND EXTERNAL FORCE

Marco Amabili
Department of Mechanical Engineering
McGill University
817 Sherbrooke Street West
Montreal, Quebec, H3A 2K6
marco.amabili@mcgill.ca

Kostas Karagiozis
Department of Mechanical Engineering
McGill University
817 Sherbrooke Street West
Montreal, Quebec, H3A 2K6
konstantinos.karagiozis@mcgill.ca

Michael P. Païdoussis
Department of Mechanical Engineering
McGill University
817 Sherbrooke Street West
Montreal, Quebec, H3A 2K6
mary.fiorilli@mcgill.ca

ABSTRACT

This study treats the nonlinear behaviour of cylindrical shells subjected to internal fluid flow and to an external periodic transverse point force. The shell is supported at both ends by axial and rotational springs capable of simulating boundary conditions ranging from clamped to simple supports. This complex boundary condition configuration is preferred in our analysis in order to be able to compare theoretical findings with water-tunnel experiments available in the literature. The external concentrated point force is applied at mid-length of the immersed shell structure acting in the radial direction and the excitation frequency values lie within the spectral neighbourhood of one of the shell's lowest frequencies for different flow velocities. The structural model is based on the full nonlinear Donnell shell equations of motion including the effect of the in-plane inertia and accounting for geometric imperfections. The fluid is assumed to be incompressible and inviscid and the flow isentropic and irrotational; it is modelled using potential flow theory with the addition of unsteady viscous terms obtained from the time-averaged Navier-Stokes equations. The coupled system is discretized using a solution expansion based on trigonometric functions satisfying the shell boundary conditions exactly. Numerical results show the nonlinear response at different flow velocities for (i) a fixed excitation amplitude and variable excitation frequency, and (ii) fixed excitation frequency varying the excitation amplitude. Bifurcation diagrams of Poincaré maps obtained from direct time integration are presented, as well as the maximum Lyapunov exponent, in order to classify the system dynamics. In particular, periodic, quasi-periodic, sub-harmonic and chaotic responses have been detected. The full spectrum of the Lyapunov exponents and the Lyapunov dimension have been calculated for the chaotic response; they reveal the occurrence of large-dimension hyperchaos.

1. INTRODUCTION

Large amplitude vibrations of thin shells containing fluids are a major safety concern due to excitations of many kinds, including flow excitation. In the early studies, linear shell theory has been used to describe the oscillation of thin shells, which is accurate only for vibration amplitudes significantly smaller than the shell thickness.

Païdoussis and Denise [1] presented one of the first complete studies on the dynamics of shells conveying fluid for both clamped and cantilevered shells subjected to axial flow; a travelling wave type solution was utilized, nevertheless satisfying the pertinent boundary conditions, along with a separation of variables method to solve the boundary value problem for linear fluid-structure interaction. Additional studies by Weaver and Unny [2], utilizing the Fourier transform method predicted similar results for the stability of simply supported shells. Païdoussis et al. [3] extended this method to coaxial cylindrical shells. Another interesting study on the effect of the boundary conditions at the shell ends was presented by Horáček and Zolotarev [4]. In these four papers [1-4], not only shell stability but also the linear dependence of the natural frequencies of the system on the flow velocity are investigated.

The literature related to nonlinear studies of shells coupled to flowing fluid is not large. Selmane and Lakis [5] studied the large amplitude vibration of shells with flow. They considered the nonlinear free vibrations of open and closed circular cylindrical shells with fluid flow by using a hybrid finite element method. The formulation is based on the nonlinear Sanders-Koiter shell theory, so that structural nonlinearities are taken into account. Results have been obtained for the free nonlinear vibrations of an open circular cylindrical shell with flowing fluid.

In a recent series of papers, Amabili, Pellicano and Païdoussis [6-9] systematically studied the nonlinear dynamics and large-amplitude vibrations of simply supported, circular cylindrical shells, with and without quiescent or flowing fluid, by using as a basis the eigenfunctions of a simply supported beam. Moreover, the convergence of the solution was studied in Refs. [7, 8]. Amabili [10] investigated the effect of geometric imperfections and compared calculations and experiments, thus validating the theory. More accurate shell theories have been used by Amabili [11] to study the same problem. Results show that, for water-filled shells, Donnell's nonlinear shallow-shell theory gives reasonably accurate results, provided n is not too small.

Not many studies on shells with clamped boundary conditions, empty or filled with fluid, subjected to external harmonic excitation are available due to the numerical problems related to satisfying the physical boundary conditions. Matsuzaki and Kobayashi [12] studied theoretically and experimentally the large-amplitude vibrations of clamped circular cylindrical shells using the Donnell nonlinear shallow shell theory predicting a softening type of nonlinear response. Chiba [13] conducted an experimental study of large-amplitude vibrations of clamped shells partially filled with water to different levels. The results indicated that when the shells are partially filled a more pronounced nonlinear response is produced. Amabili [14] investigated the nonlinear vibrations of circular shells with different boundary conditions subjected to radial harmonic excitation in the spectral neighbourhood of the lowest resonances; geometric imperfections were taken into account. Karagiozis et al. [15] presented two different theoretical models for the nonlinear oscillations of clamped shells, empty or fully filled with water, subjected to external harmonic excitation. Both models predicted, with excellent accuracy, the softening nonlinear response obtained in the experiments conducted by Chiba [13]. Additional case studies are included in Amabili [16].

In the present study the nonlinear stability of an aluminium shell clamped at both ends, subjected to internal water flow and to an external radial harmonic excitation in the spectral neighbourhood of one of the lowest natural frequencies, is investigated for different flow velocities. Karagiozis et al. [17] and Amabili et al. [18] investigated the nonlinear response of the same shell system subjected only to internal fluid flow, generating results in excellent agreement with the experimental results of Karagiozis [19]. Bifurcation diagrams of Poincaré maps obtained from direct time integration and calculation of the maximum Lyapunov exponent have been used to study the system. By increasing the excitation amplitude, the periodic solution changes to chaotic response.

2. THEORY

The shell model consists of a circular cylindrical shell of length L, mean radius R, and thickness h, such that $h/R \ll 1$, shown in Fig.1. The origin of the cylindrical coordinate system, $(O;\ x, r, \theta)$, is positioned at the centre of one end of the shell. The shell is assumed to be of homogeneous, isotropic elastic material of Young's modulus E and Poisson ratio ν. The displacements of the shell middle surface are denoted by u, v and w, in the axial, circumferential and radial directions, respectively; w is taken positive outward.

The following boundary conditions are imposed at the shell ends:

$$v = w = w_0 = 0, \qquad \text{at } x = 0, L, \qquad \text{(1a-c)}$$

$$N_x = -k_a\, u, \qquad \text{at } x = 0, L, \qquad \text{(1d)}$$

$$M_x = -k_r\, (\partial w/\partial x), \qquad \text{at } x = 0, L, \qquad \text{(1e)}$$

where N_x is the axial load per unit length, M_x is the bending moment per unit length, k_a is stiffness per unit length of the elastic, distributed axial springs at x = 0 and L and k_r is the stiffness per unit length of the elastic, distributed rotational springs at x = 0 and L. Moreover, u, v and w must be continuous in θ. The boundary conditions (1a,b) restrain the radial and circumferential shell displacements at both edges. Equation (1d) gives and elastic axial constraint at the shell edges.

Different values of the axial spring k_a are assume for asymmetric and axisymmetric deformation modes in the numerical calculations in order to simulate experimental boundary conditions.

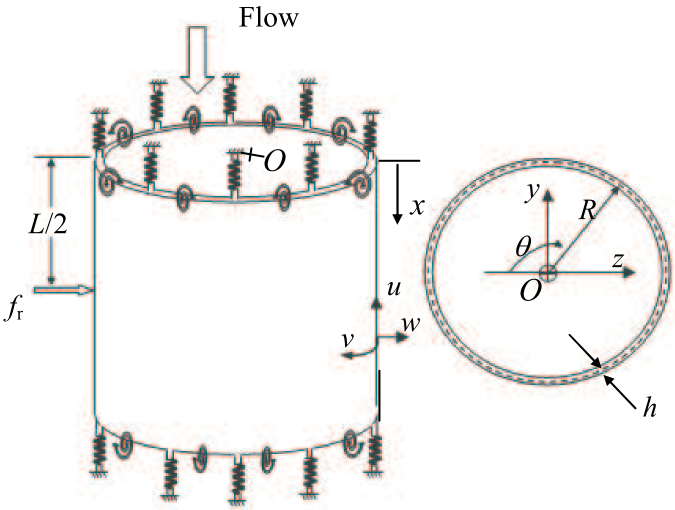

FIGURE 1. Shell geometry and boundary conditions

A base of shell displacements is used to discretize the system; the displacements u, v and w can be expanded by using the following expressions, which identically satisfy boundary conditions (1a,b):

$$u(x,\theta,t)=\sum_{m=1}^{5}\left[u_{m,n,c}(t)\cos(n\theta)+u_{m,n,s}(t)\sin(n\theta)\right]\cos(\lambda_m x)+\sum_{m=1}^{3}u_{m,2n,c}(t)\cos(2n\theta)\cos(\lambda_m x)+\sum_{m=1}^{4}u_{2m-1,0}(t)\cos(\lambda_{2m-1}x), \tag{2a}$$

$$v(x,\theta,t)=\sum_{m=1}^{5}\left[v_{m,n,c}(t)\sin(n\theta)+v_{m,j,s}(t)\cos(n\theta)\right]\sin(\lambda_m x)+\sum_{m=1}^{4}v_{m,2n,c}(t)\sin(2n\theta)\sin(\lambda_m x), \tag{2b}$$

$$w(x,\theta,t)=\sum_{m=1}^{3}\left[w_{m,n,c}(t)\cos(n\theta)+w_{m,n,s}(t)\sin(n\theta)\right]\sin(\lambda_m x)+\sum_{m=1}^{4}w_{2m-1,0}(t)\sin(\lambda_{2m-1}x), \tag{2c}$$

where j is the number of circumferential waves, m is the number of longitudinal half-waves, $\lambda_m = m\pi/L$, and t is the time; $u_{m,j}(t)$, $v_{m,j}(t)$ and $w_{m,j}(t)$ are the generalized coordinates, which are unknown functions of t; the additional subscript c or s indicates if the generalized coordinate is associated with cosine or sine function in θ, except for v, for which the notation is reversed (no additional subscript is used for axisymmetric terms). More terms in the expansion are necessary for in-plane than for radial displacements. Denoting with n the number of circumferential waves in the shape of the buckled mode, terms with j = 2n and 3n circumferential waves can be added to expansion, but they do not play an important role if geometric imperfections are not introduced.

Imperfections are expanded in the following Fourier series

$$w_0(x,\theta,t)=\sum_{m=1}^{\hat{M}}\sum_{j=0}^{\hat{N}}\left[A_{m,n}\cos(j\theta)+B_{m,n}\sin(j\theta)\right]\times\sin(m\pi x/L). \tag{3}$$

2.1 Fluid-structure interaction

The shell is assumed to be positioned within a large concentric solid tube filled with quiescent fluid to include the effect of the inertia of the surrounding fluid. The contained flowing fluid and the external quiescent fluid are assumed to be incompressible and inviscid and the flow isentropic and irrotational, so that potential theory can be used to describe fluid motion. The fluid model is based on the Païdoussis and Denise model [20]. Moreover, the steady-state viscous effects are added in the fluid model separately. These effects are evaluated using the time averaged Navier-Stokes equations.

Liquid-filled shells vibrating in the low-frequency range satisfy the incompressibility hypothesis very well. Nonlinear effects in the dynamic pressure and in the boundary conditions at the fluid-structure interface are neglected. The shell prestress due to the fluid weight is also neglected. The fluid motion is described by the velocity potential Φ, which satisfies the Laplace equation. The velocity potential is related to the scalar potential function by $\Psi=Ux+\Phi$. Both ends of the fluid volume (corresponding to the shell edges) are assumed to be open, so that a zero pressure is assumed there; this physically corresponds to a long shell periodically supported (e.g. with ring stiffeners) or it approximates a can closed by very thin circular plates.

If no cavitation occurs at the fluid-shell interface, the boundary condition expressing the contact between the shell wall and the flow is

$$\left(\frac{\partial \Phi}{\partial r}\right)_{r=R}=\left(\frac{\partial w}{\partial t}+U\frac{\partial w}{\partial x}\right). \tag{4}$$

By using the method of separation of variables, Φ has the following form:

$$\Phi=\sum_{m=1}^{M}\sum_{n=0}^{N}\frac{L}{m\pi}\frac{\mathrm{I}_n(m\pi r/L)}{\mathrm{I}'_n(m\pi R/L)}\left(\frac{\partial w_{m,n}}{\partial t}+U\frac{\partial w_{m,n}}{\partial x}\right) \tag{5}$$

2.2 Energy associated with flow

By using the Green's theorem, the total energy associated with the flow is given by

$$E_{TF}=\frac{1}{2}\rho_F\iiint_{\Gamma}\mathbf{v}\cdot\mathbf{v}\,\mathrm{d}\Gamma=\frac{1}{2}\rho_F\iiint_{\Gamma}\nabla\Psi\cdot\nabla\Psi\,\mathrm{d}\Gamma$$

$$=\frac{1}{2}\rho_F \iint_{\Omega} \left(\Psi \frac{\partial \Psi}{\partial \nu} \right)\bigg|_{\Omega} \, \mathrm{d}\Omega , \tag{6}$$

where Γ and Ω are the cylindrical fluid volume inside the shell (delimited by the length L) and the boundary surface of this volume, respectively, and ν is the coordinate along the normal to the boundary, taken positive outward. Equation (6) shows that the energy E_F can be conveniently divided into three terms having different contributions of time functions and their derivatives:

$$E_F = T_F + E_G - V_F . \tag{7}$$

The first and second of the three terms on the right-hand side can be identified as the kinetic and gyroscopic energies, respectively; an opposite sign is introduced for the potential energy V_F for convenience. The time-mean Navier-Stokes equations [18] are employed to calculate the fluid steady viscous effects assuming that the flow is fully turbulent. The unsteady viscous forces [21] are neglected in this investigation.

2.3 Generalized forces

In this analysis, the shell is subjected not only to flowing fluid but also to an external harmonic force excitation active only in the radial direction, as indicated in Figure 1. The external localized (point) force on the shell surface is directed inwards and is applied at a point $\left(\tilde{x},\tilde{\theta}\right)$. The excitation force in the radial direction has the following general form

$$f_r = \tilde{f}\,\delta(R\theta - R\tilde{\theta})\,\delta(x-\tilde{x})\cos(\omega t), \tag{8}$$

where δ is the Dirac delta function, and $\tilde{f}$ is the magnitude of point force. It is important to note that in the present analysis the driving frequency (excitation frequency) is chosen to have values close to the natural frequency of the lowest modes of the shell.

The virtual work W done by the external force is written as

$$W = \tilde{f}\cos\left(\omega t\right)\left(w\right)_{x=L/2,\ \theta=0} . \tag{9}$$

Damping is considered to arise strictly within the shell material. It is assumed to be of the viscous type and is taken into account by using Rayleigh's dissipation function [20].

The generalized forces Q_j are obtained by differentiation of the Rayleigh dissipation function F and of the virtual work W done by external forces:

$$Q_j = -\frac{\partial F}{\partial \dot{q}_j} + \frac{\partial W}{\partial q_j}, \tag{10}$$

where $\partial F / \partial \dot{q}_j = c_j \, \dot{q}_j$ and c_j is the dissipation coefficient that has a different value for each mode.

2.4 Lagrange equations of motion

The following notation is introduced:

$$\mathbf{q} = \left\{u_{m,n,c}, u_{m,n,s}, v_{m,n,c}, v_{m,n,s}, w_{m,n,c}, w_{m,n,s}\right\}^{\mathrm{T}},$$
$$m = 1,\ldots,M_1 \text{ or } M_2 \text{ and } n = 0,\ldots,N . \tag{11}$$

The generic element of the time-dependent vector $\mathbf{q}$ is referred to as q_j. The dimension of $\mathbf{q}$ is $\bar{N}$, which is the number of degrees of freedom (dofs) used in the mode expansion.

In the present case, the Lagrange equations of motion are rewritten as

$$\frac{\mathrm{d}}{\mathrm{d}t}\left[\frac{\partial (T_S + T_F)}{\partial \dot{q}_j}\right] - 2\frac{\partial E_G}{\partial q_j} + \frac{\partial (U_S + V_F)}{\partial q_j} = Q_j ,$$
$$j = 1,\ldots,\bar{N} . \tag{12}$$

2.5 Equation of motion

The equations of motion have been obtained by using the Mathematica 4 computer software [22], in order to perform analytical integrals of trigonometric functions. The generic j^{th} Lagrange equation is divided by the modal mass associated with $\ddot{q}_j$ and is then transformed into the following two first-order equations by using the dummy variable y_j:

$$\begin{cases} \dot{q}_j = y_j , \\ \dot{y}_j = -2\zeta_j \omega_j y_j - \sum_{i=1}^{\text{dofs}} z_{j,i} q_i - \sum_{i=1}^{\text{dofs}}\sum_{k=1}^{\text{dofs}} z_{j,i,k} q_i q_k - \\ \quad \sum_{i=1}^{\text{dofs}}\sum_{k=1}^{\text{dofs}}\sum_{l=1}^{\text{dofs}} z_{j,i,k,l} q_i q_k q_l + f\cos\left(\omega t\right), \quad \text{for } j = 1\ldots\text{dofs}, \end{cases} \tag{13}$$

where f=0 if $q_j = u_{m,j,s}\left(t\right)$ and coefficients z have long expressions that include also geometric imperfections.

The resulting first-order nonlinear nondimensionalized differential equations are studied by using (i) the software AUTO 97 [23] for continuation and bifurcation analysis of nonlinear ordinary differential equations, and (ii) direct integration of the equations of motion by using the DIVPAG routine of the Fortran library IMSL. The AUTO 97 software is capable of continuation of the solution, bifurcation analysis and branch switching by using arclength continuation and collocation methods. In particular, the shell response under harmonic excitation has been studied by using an analysis in two steps: (i) first the excitation frequency has been fixed far enough from resonance and the magnitude of the excitation has been used as bifurcation parameter; the solution has been started at zero force (where the solution is the trivial undisturbed configuration of the shell) and it has been continued upwards to reach the desired force magnitude; (ii) then, the solution was continued by using the excitation frequency as bifurcation parameter.

Direct integration of the equations of motion by using Gear's BDF method (routine DIVPAG of the Fortran library IMSL) has also been performed to check the results and obtain the time behaviour. The Adams-Gear algorithm was used due to the relatively high dimension of the dynamical system.

2.6 Maximum Lyapunov exponent and dimension

In order to evaluate the maximum Lyapunov exponent, which is useful to characterize regular or chaotic motion of the shell, it is necessary to assume a reference trajectory $\mathbf{x}_r(t)$ in the phase plane $(\mathbf{q}, \dot{\mathbf{q}}$ plane$)$ and observe a neighbouring trajectory originated at infinitesimal initial perturbation $\delta\mathbf{x}(t_0)$ from the reference trajectory (see Argyris et al. [24]). The evolution of the perturbation during time, $\delta\mathbf{x}(t)$, is governed by the following variational equations:

$$\begin{cases} \dfrac{\mathrm{d}}{\mathrm{d}t}\delta q_j = \delta y_j \\ \dfrac{\mathrm{d}}{\mathrm{d}t}\delta y_j = -2\zeta_j\omega_j\delta y_j - \sum_{i=1}^{\mathrm{dofs}} z_{j,i}\delta q_i - \sum_{i=1}^{\mathrm{dofs}}\sum_{k=1}^{\mathrm{dofs}} z_{j,i,k}\delta q_n\left(\delta_{k,n}q_i + \delta_{i,n}q_k\right) \\ -\sum_{i=1}^{\mathrm{dofs}}\sum_{k=1}^{\mathrm{dofs}}\sum_{l=1}^{\mathrm{dofs}} z_{j,i,k,l}\delta q_n\left(\delta_{k,n}q_k q_l + \delta_{k,n}q_i q_l + \delta_{l,n}q_k q_i\right) \text{ for } j = 1\ldots\mathrm{dofs}, \end{cases} \tag{14}$$

where $\delta_{k,n}$ is the Kronecker delta. Taking δq_j and δy_j as new variables, the simultaneous integration of the $4\times$ dofs first-order differential equations has been performed (equations (13) are nonlinear and are integrated by using DIVPAG IMSL routine, and equations (14) are linear, but with time-varying coefficients, and are integrated by using the adaptive step-size 4th/5th order Runge-Kutta method). The excitation period has been divided into 104 integration steps in order to have accurate evaluation of the time-varying coefficients in equations (14) that are obtained at each step by integration of equations (13). To find a reference trajectory, sufficient steps are taken to eliminate the transient for both sets of equations (13) and (14). Then, 1×10^6 steps are used for evaluation of the maximum Lyapunov exponent for the reference trajectory $\mathbf{x}_r(t)$, which is given in its simplified form by

$$\sigma_1 = \lim_{t\to\infty}\sup\frac{1}{t}\ln\left|\delta\mathbf{x}(t)\right|. \tag{15}$$

Then, by restoring at each integration time step k the amplitude of $\delta\mathbf{x}(t)$ to its original unitary measure via the re-normalisation $\delta\overline{\mathbf{x}}(t) = \delta\mathbf{x}(t)/d_k$ where $\left|\delta\mathbf{x}(t)\right|_k = d_k$, the following formula for the maximum Lyapunov exponent, evaluated at step k, is obtained:

$$\sigma_{1,k} = \frac{1}{k\,\Delta t}\sum_{i=1}^{k}\ln d_i\,. \tag{16}$$

In the numerical calculation of the maximum Lyapunov exponent, the non-dimensional time previously introduced has been used.

The Fortran computer program developed to calculate $2\times$ dofs numbers designating the spectrum of the Lyapunov exponents is described in reference [25] and has been properly validated.

The long-term behaviour of dissipative systems is characterized by attractors with different characteristics if the trajectories are not drawn towards infinity. After a transient state, in which some modes of motion finally vanish due to damping, the state of the system approaches an attractor where the number of independent variables, which determine the dimension of the phase space, is generally reduced considerably [18]. The fractal dimension is a measure of the strangeness of an attractor and indicates the number of effective independent variables determining the long-term behaviour of a motion. There exist several measures of the fractal dimension, including the well-known Lyapunov dimension, which is defined as [25]

$$d_L = s + \sum_{r=1}^{s}\sigma_r\Big/\left|\sigma_{s+1}\right|, \tag{15}$$

where the Lyapunov exponents are ordered by their magnitude, and s is obtained by satisfying the following conditions:

$$\sum_{r=1}^{s}\sigma_r > 0 \text{ and } \sum_{r=1}^{s+1}\sigma_r < 0\,. \tag{16}$$

3. NUMERICAL RESULTS

This numerical analysis is an extension of the study presented by Karagiozis et al. [17] and Amabili et al. [18] that compared succesfully numerical models with the experimental results of Karagiozis [19]. The aluminium shell is assumed to have the following dimensions and material properties: L=0.1225; R=0.041125; h=0.000137 m; ρ_s=2720 $\mathrm{kg/m^3}$; ν=0.33 and $E=70\times10^9$ Pa;. The assumed stiffness of axial and rotational springs distributed around the shell ends at x = 0 and L are $k_{a1}=1\times10^7$ N/m^2, $k_{a2}=1\times10^5$ N/m^2 and $k_r=0.3\times10^3$ N/rad. The axial springs k_{a1} that restrain asymmetric modes are more rigid than k_{a2} which are set to restrain the axiasymmetric modes. In the experiments the shell was glued with epoxy to solid rings at the boundaries, represented here by springs with stiffness k_{a1}, but the rings were also connected to the water tunnel using a softer silicone material, represented by springs with stiffness k_{a2}. Therefore, the shell boundary conditions lie between simply supported and clamped ends. The assumed fluid (conveyed and quiescent in the external confinement) is water with mass density $\rho_F = 1000\ \mathrm{kg/m^3}$. The quiescent fluid in the external space was confined by a rigid cylinder with internal radius of 0.1015 m. A nondimensional fluid velocity V is introduced for convenience, defined as in Weaver and Unny [2] $V = U\Big/\left\{\left(\pi^2/L\right)\left[D/(\rho h)\right]^{1/2}\right\}$, where U is the flow velocity and $D = E h^3/[12(1-\nu^2)]$.

The critical wavenumber observed in the experiments is n=6, with quite a regular shape (see Karagiozis [19] and Karagiozis et al. [26]); calculations confirm that this is the first mode reaching divergence. Therefore, all the results shown here are for n=6. The damping ratio $\zeta_{1,6}$ used in the calculations was set to 0.005. In addition, the solution expansion involved forty-two symmetrical driven and companion modes.

3.1 Stability analysis and periodic response

Figure 2 shows the stability diagram for the aluminium shell in a bifurcation plot of the amplitude of the first generalized coordinate $w_{1,6,c}$ versus the non-dimensional flow velocity. As the flow velocity increases, the shell remains undeformed until the pitchfork bifurcation at V=3.69, at which point the system loses stability by static divergence according to linear theory. The solution bifurcates into two unstable branches; these branches fold at V=1.28 and become stable thereafter. As shown for the first time in Amabili et al. [6] for simply-supported shells, and later by Karagiozis et al. [17] for clamped shells, there is a range of flow velocities between the point of the linear onset of instability and the folding point in which the shell may jump from its undeformed state to a deformed state of large amplitude if sufficiently perturbed. The perturbation may be in the form of an external force acting on the shell wall or it may be a flow perturbation. In our case, this critical flow range is quite enormous: over 65% of the range ($1.28 \le V \le 3.69$) from zero flow velocity to the point of linear loss of stability!

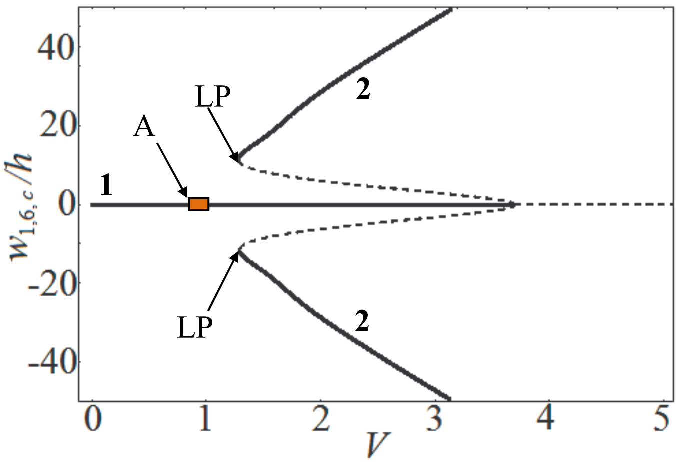

FIGURE 2: Bifurcation diagram of the non-dimensional amplitude of the first driven mode $w_{1,6,c}/h$ versus the non-dimensional flow velocity V of a clamped aluminium shell with internal water flow: ———— , Stable solution branches; – – – -, unstable solution branches. A is the point of interest with V=1 and LP are the limit points of the solution branches.

To further study the forced response of the aluminium shell, point A on the bifurcation diagram is chosen to be investigated. Here the forced response is obtained spanning the frequency range around the fundamental resonance. Point A lies before the folding points (LP in Figure 2), thus only one stable solution on branch 1 exists, namely that of zero shell deformation. The response-frequency relationship of the fundamental mode for a shell subjected to water flow and a harmonic excitation of magnitude 0.0165 N at $\tilde{x} = L/2$ and $\tilde{\theta} = 0$ is shown in Figures 3(a,b). In all cases the shell exhibits a softening type of nonlinearity that is more pronounced as the flow velocity is increased. As the frequency of excitation is increased the solution loses stability by a pitchfork bifurcation. This pitchfork bifurcation point gives rise to unstable solutions for branch 1, where only the driven mode is active (the companion mode is zero). It also gives rise to an initially stable branch 2 with companion mode participation (as shown in Figure 3(b)). It is interesting to note that the stable Branch 2 loses stability through two Neimark-Sacker (torus) bifurcations The shell behaviour is complicated, as secondary Neimark-Sacker bifurcation points exist along the stable periodic solutions, producing periodic and quasi-periodic oscillations on branch 2. As the flow velocity increases, the region for quasi-periodic responses also increases.

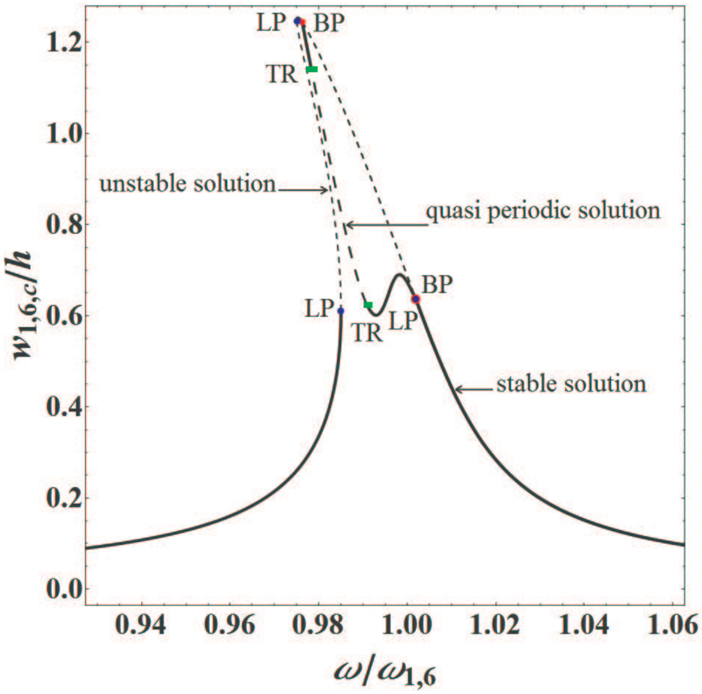

(a)

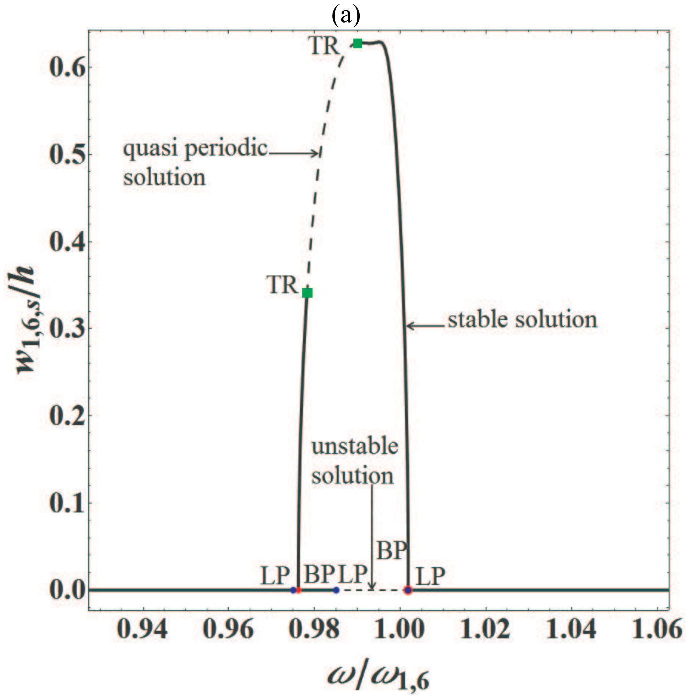

(b)

FIGURE 3. Maximum amplitude of vibration of the first asymmetric mode versus the excitation frequency for three different values of the nondimensional velocity and a force amplitude equal to 12.5[N]. ————, stable solution; – – – –, quasi-periodic solution; ··············· , unstable solution; ■, Torus bifurcation points; ●, bifurcation points. (a) Maximum amplitude of the first driven asymmetric modes versus the excitation frequency; (b) maximum amplitude for the first asymmetric companion modes versus the excitation frequency.

It is also noted that, as the flow velocity increases, the quasi-periodic solution branch (Branch 2 between the two torus bifurcation points) interferes with the unstable Branch 1 (unstable solution between the limit points) allowing for amplitude-modulated responses. These results were obtained using the AUTO 97 software package.

3.2 Stability analysis and periodic response

In this section the response of the shell for the flow condition at point A (see Fig.2, *V*=1) was investigated by increasing the force amplitude from 0 to 17 N while keeping the frequency of excitation at $\omega/\omega_{1,6} = 1.00$. Specifically, the DIVPAG Fortran routine was used to integrate the equations of motion when *V*=1 with 200 frequency steps; at each step, a Poincaré map and the maximum Lyapunov exponent were calculated. This required a large computational effort, and the computer codes had to be optimized for speed, computational cost and accuracy.

The rich dynamics of the response is shown in Fig. 4(a) below. The results in Figure 4(a) for the first driven mode show that there is a complex periodic response with jumps and phase changes along with sub-harmonic responses for low excitation values. The first companion mode goes through similar intervals of sub-harmonic response for low excitation load values. For higher excitation values the system becomes chaotic. The second asymmetric mode, $w_{2,6,c}(t)$, is activated when the system becomes chaotic. Therefore, for flow conditions at point A (*V*=1), both driven and companion components of the first and second modes are very active, contributing large displacements when the system experiences chaos. The presence of a flowing fluid amplifies the complexity of the system response.

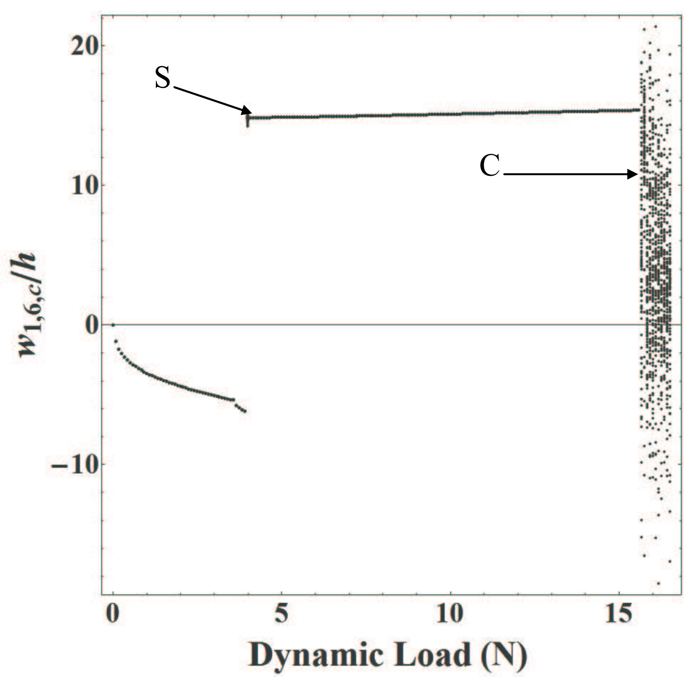

(a)

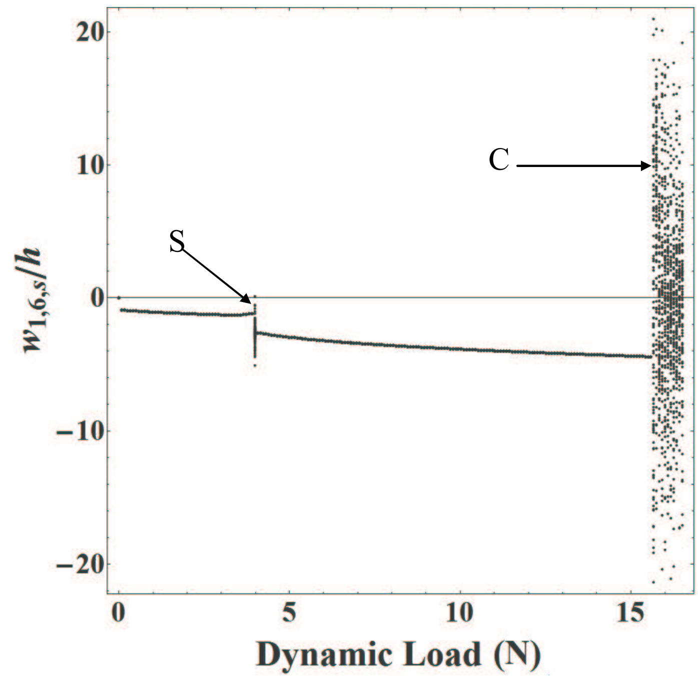

(b)

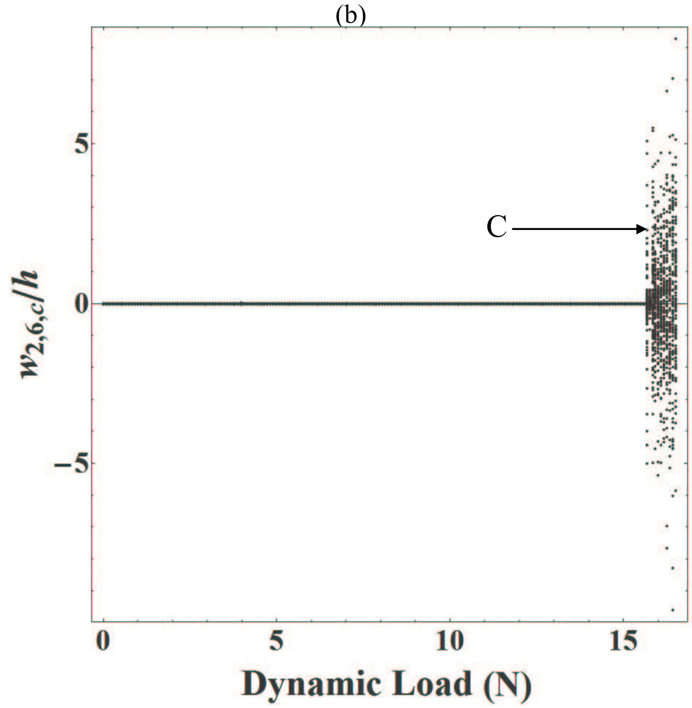

(c)

FIGURE 4: Bifurcation diagram of Poincaré points for increasing force amplitude from $\tilde{f}$ =0 to 17.0 N, with $\omega/\omega_{1,6} = 1.0$ and *V*=1. (a) Bifurcation diagram for the driven mode; (b) bifurcation diagram of the companion mode; (c) bifurcation diagram of the second driven mode. S denotes sub-harmonic responses and C denotes the chaotic response of the system.

The chaotic nature of the system can be seen in Figure 5(a), in a plot of the maximum Lyapunov exponent versus the excitation force magnitude. For $\tilde{f}$ =15.67 N the Lyapunov exponent becomes very large and positive. The Poincaré map is shown in Figure 5(b) for $\tilde{f}$ =11.99 N.

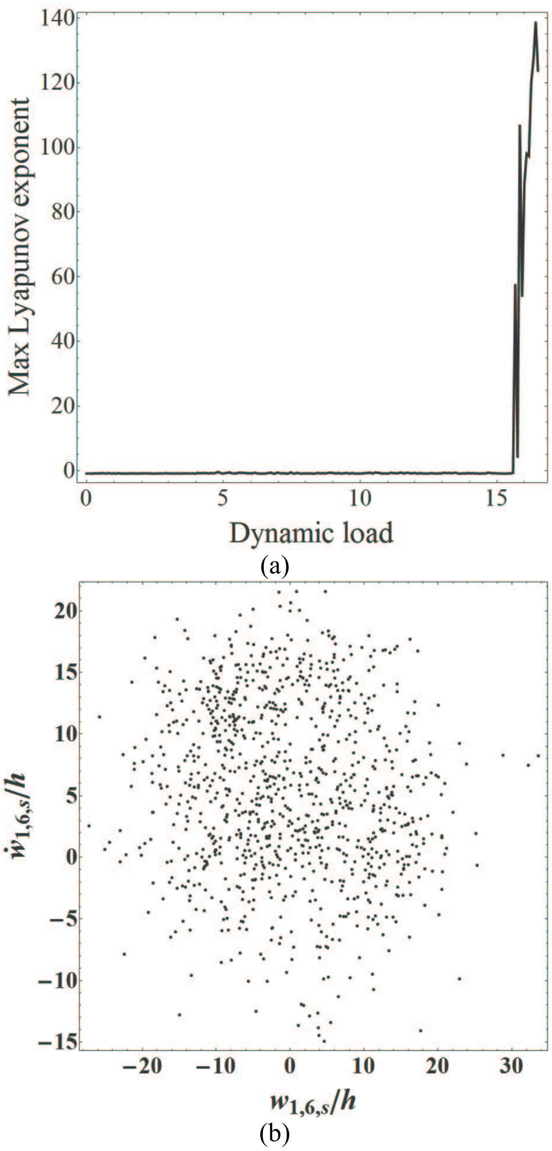

FIGURE 5: Bifurcation diagrams and Poincaré maps for the fundamental driven mode when the force $\tilde{f}$ is increased to 17.0 N, with $\omega/\omega_{1,6}=1.0$ and V=1. (a) Dynamic load versus the maximum Lyapunov exponent; (b) Poincaré map for the fundamental driven mode for $\tilde{f}$ =11.99 N.

4. CONCLUSIONS

This paper summarizes the complex dynamical behaviour of shells conveying fluid under external radial harmonic excitation. It was shown that periodic, sub-harmonic and chaotic responses are possible, depending on the flow velocity, amplitude and frequency of the harmonic excitation.

The present study showed that when the flow velocity is nonzero the second asymmetric mode significantly contributes in the chaotic oscillations of the excited shell. This model is a first successful step in the development of reliable semi-analytical methods with low computational cost to describe the nonlinear behaviour of clamped shells conveying fluid and excited by a harmonic force.

ACKNOWLEDGEMENT

The authors would like to thank NSERC of Canada for providing financial support for this research.

REFERENCES

[1] Païdoussis, M.P., Denise, J.P., 1972, “Flutter of thin cylindrical shells conveying fluid”, *Journal of Sound and Vibration*, **20**, pp. 9-26.

[2] Weaver, D.S., Unny, T.E., 1973, “On the dynamic stability of fluid-conveying pipes”, *Journal of Applied Mechanics*, **40**, pp. 48-52.

[3] Païdoussis, M.P., Chan, S. P., Misra, A.K., 1984, Dynamics and stability of coaxial cylindrical shells containing flowing fluid”, *Journal of Sound and Vibration*, **97**, pp. 201-235.

[4] Horáček, J., Zolotarev, I., 1984, “Influence of fixing edges of a cylindrical shell with conveying fluid on its dynamic characteristics”, *Soviet Applied Mechanics*, **20**, pp. 756-765.

[5] Selmane A., Lakis, A.A., 1997, “Non-linear dynamic analysis of orthotropic open cylindrical shells subjected to a flowing fluid”, *Journal of Sound and Vibration*, **202**, pp. 67-93.

[6] Amabili, M., Pellicano, F., Païdoussis, M. P., 1999, “Non-linear dynamics and stability of circular cylindrical shells containing flowing fluid. Part I: stability”, *Journal of Sound and Vibration*, **225**, pp. 655-699.

[7] Amabili, M., Pellicano, F., Païdoussis, M. P., 1999, “Non-linear dynamics and stability of circular cylindrical shells containing flowing fluid, Part II: large-amplitude vibrations without flow”, *Journal of Sound and Vibration*, **228**, pp. 1103-1124.

[8] Amabili, M., Pellicano, F., Païdoussis, M. P., 2000, “Non-linear dynamics and stability of circular cylindrical shells containing flowing fluid. Part III: truncation effect without flow and experiments”, *Journal of Sound and Vibration*, **237**, pp. 617-640.

[9] Amabili, M., Pellicano, F., Païdoussis, M.P., 2000, “Non-linear dynamics and stability of circular cylindrical shells containing flowing fluid. Part IV: large-amplitude vibrations with flow”, *Journal of Sound and Vibration*, **237**, pp. 641-666.

[10] Amabili, M., 2003, "Theory and experiments for large-amplitude vibrations of empty and fluid-filled circular cylindrical shells with imperfections", *Journal of Sound and Vibration*, **262**, pp. 921-975.

[11] Amabili, M., 2003, "Comparison of shell theories for large-amplitude vibrations of circular cylindrical shells: Lagrangian approach", *Journal of Sound and Vibration*, **264**, pp. 1091-1125.

[12] Matsuzaki, Y., Kobayashi, S., 1969, "A theoretical and experimental study of the nonlinear flexural vibration of thin circular shells with clamped ends", *Transactions of the Japan Society for Aeronautical and Space Sciences*, **12**, pp. 55-62.

[13] Chiba, M., 1993, "Experimental studies on a nonlinear hydroelastic vibration of a clamped cylindrical tank partially filled with liquid", *ASME Journal of Pressure Vessel Technology*, **115**, pp. 381-388.

[14] Amabili, M., 2003, "Nonlinear vibrations of circular cylindrical shells with different boundary conditions", *AIAA Journal*, **41**, pp. 1119-1130.

[15] Karagiozis, K.N., Amabili, M., Païdoussis, M.P., Misra, A.K., 2005, "Nonlinear vibration of fluid-filled clamped circular shells, *Journal of Fluids and Structures*, **21**, pp. 579-595.

[16] Amabili, M., 2008. *Nonlinear Vibrations and Stability of Shells and Plates*, Cambridge University Press, New York, USA.

[17] Karagiozis, K.N., Païdoussis, M.P., Amabili, M., Misra, A.K., 2008, "Nonlinear stability of cylindrical shells subjected to axial flow: Theory and experiments", *Journal of Sound and Vibration*, **309**, pp. 637-676.

[18] Amabili, M., Karagiozis, K., Païdoussis, M.P., 2009, "Effect of geometric imperfections on non-linear stability of circular cylindrical shells conveying fluid", *International Journal of Non-Linear Mechanics*, **44**, pp. 276-289.

[19] Karagiozis, K.N., 2006, *Experiments and theory on the nonlinear dynamics and stability of clamped shells subjected to axial fluid flow or harmonic excitation*, Ph.D. Thesis, McGill University, Montreal, Canada.

[20] Païdoussis, M.P., Denise, J.P., 1972. "Flutter of thin cylindrical shells conveying fluid". *Journal of Sound and Vibration* **20**, pp. 9–26.

[21] Païdoussis,M.P., 2003. Fluid Structure Interaction: Slender Structures and Axial Flow*, Vol. 2.* London: Elsevier Academic Press.

[22] Wolfram, S., 1999, *The Mathematica Book*, 4th edition, Cambridge University Press, Cambridge, UK.

[23] Doedel, E.J., Champneys, A.R., Fairgrieve, T.F., Kuznetsov, Y.A., Sandstede, B., Wang, X., 1998, *AUTO 97: Continuation and Bifurcation Software for Ordinary Differential Equations (with HomCont)*, Concordia University, Montreal, Canada.

[24] Argyris, J., Faust, G., Haase, H., 1994, *An Exploration of Chaos*, North-Holland, Amsterdam.

[25] Amabili, M., 2005, "Non-linear vibrations of doubly curved shallow shells", *International Journal of Non-Linear Mechanics*, **40**, pp. 683-710.

[26] Karagiozis, K.N., Païdoussis, M.P., Misra, A.K., Grinevich, E., 2005, "An experimental study on the nonlinear dynamics of cylindrical shells with clamped ends subjected to axial flow", *Journal of Fluids and Structures*, **20**, pp. 801-816.